Solving the Conundrum of Active Site Density of PGM-free ORR Catalysts in situ Fuel Cells Using Fourier Transform Alternating Current Voltammetry

Rifael Snitkoff
Bar Ilan University
Ariel Friedman
Bar Ilan University https://orcid.org/0000-0002-2453-9428
Yan Yurko
Bar Ilan University
Piotr Zelenay
Los Alamos National Laboratory https://orcid.org/0000-0002-8962-9520
Alan Bond
Monash University
Lior Elbaz (lior.elbaz@hotmail.com)
Bar Ilan University https://orcid.org/0000-0003-4989-5135

Article

Keywords: fuel cells, PGM-free ORR catalysts, Fourier-transformed alternating current voltammetry

Posted Date: April 15th, 2021

DOI: https://doi.org/10.21203/rs.3.rs-378185/v1

Version of Record: A version of this preprint was published at Nature Catalysis on February 24th, 2022.
See the published version at https://doi.org/10.1038/s41929-022-00748-9.

Solving the Conundrum of Active Site Density of PGM-free ORR Catalysts *in situ* Fuel Cells Using Fourier Transform Alternating Current Voltammetry

Rifael Z. Snitkoff[1], Ariel Friedman[1], Yan Yurko[1], Piotr Zelenay[2], Alan M. Bond[3] and Lior Elbaz[1,2,4*]

[1]Bar-Ilan University, Ramat-Gan 5290002, Israel
[2]Los Alamos National Laboratory, Los Alamos, NM 87545, USA
[3]School of Chemistry, Monash University, Clayton, Vic. 3800, Australia
[4]Center for Micro-Engineered Materials, University of New Mexico, NM 87106, USA
[*]Corresponding author: lior.elbaz@biu.ac.il

Abstract

Advances in the development of Pt-group metal-free (PGM-free) catalysts for oxygen reduction reaction in fuel cells produced active catalysts that allow to reduce the performance gap to the incumbent Pt-based materials. However, the utilization of the state-of-the-art PGM-free catalysts in commercial applications is currently impeded by their relatively low durability. Methods designed to study catalyst degradation in operating fuel cells are critical for the understanding and ultimately solving the durability issues. This work is the first report on the use of Fourier-transformed alternating current voltammetry (FTacV) as an electrochemical method for accurately quantifying the electrochemical site density of PGM-free ORR catalysts, and following their degradation during the operation of polymer electrolyte fuel cells. Using this method we were capable of detecting changes in performance of electrochemically active species (electrocatalytic centers in this case), allowing us, for the first time, to calculate the electrochemical active site density (EASD) which is necessary for the elucidation of the degradation mechanisms of PGM-free ORR catalysts *in situ* fuel cells.

Introduction

The rising interest in polymer electrolyte fuel cells (PEFCs) technology, part of the global shift in energy production to clean sources,[1] is accompanied by efforts to drive down the cost of this technology, focusing primarily on the cathode catalyst, the most expensive PEFC component.[2] While platinum-group metal (PGM) catalysts for oxygen reduction reaction (ORR) continues to be the materials of choice, in order for the PEFC technology to become fully viable, PGMs need to either be replaced by less expensive catalysts or their quantity significantly reduced without a penalty in the overall cell performance.[3-5]

The most promising PGM-free ORR catalysts involve first-row transition metals, such as iron and cobalt,[6] incorporated in a nitrogen-doped carbon (M-N-C catalysts).[5-10] While the advancements in the M-N-C activity has been impressive, the much sought-after improvement in durability has been impeded by limited information on changes in the PGM-free catalyst activity and its degradation rate during fuel cell testing.[11,12] Currently, the degradation of PGM-free catalysts is often quantified using the low-current region of polarization curves. While this approach is well established, it neglects complications from such factors as the catalyst pore structure, membrane conductivity, ionomer content, nature of the support, and the inhomogeneity of active sites. Hence, there exists a critical need for a method with high specificity towards catalytic activity.[12]

In the case of PGM catalysts, the electrochemical active surface area (ECSA) is used as a descriptor for catalyst degradation, and the loss of ECSA is associated with various degradation mechanisms.[13] It can be easily and accurately calculated from carbon monoxide (CO) or hydrogen adsorption/desorption stripping charges.[14] ESCA can be determined

during an accelerated stress test (AST) in an operating PEFC. It quantifies degradation of Pt-based active sites *in situ* and has been playing an important role in the development of durable PGM catalysts.

In the case of PGM-free catalysts, recent studies suggest that the active site in M-N-C ORR catalysts, such as the state-of-the-art atomically dispersed (AD) FeNC, is the FeN site.[15-18] It has been also suggested that FeN sites may be electrochemically active as a consequence of the Fe(II)/Fe(III) redox couple coinciding with the onset ORR potential.[18-20] Based on the postulate that the ORR activity in these catalysts stems from the Fe(II)/Fe(III) redox couple, the electrochemical active site density (EASD) should be proportional to the electrocatalytic ORR activity in fuel cell measurements. Hence, an in-depth analysis of the electrochemical behavior of these active sites can shed light on the processes PGM-free catalysts undergo during their degradation.

Herein, we show how Fourier-transform alternating current voltammetry (FTacV) allows to de-convolute the processes taking place at the electrode and generate harmonics which can be used to calculate the EASD, and serve as activity descriptors to study *in situ* degradation processes of PGM-free catalysts in PEFCs.

Experimental

Baseline Measurements Using $[Ru(NH_3)_6]^{3+/2+}$

In almost all previous FTacV studies the measurements were conducted using homemade potentiostats specifically optimized for the technique. In this work, all electrochemical measurements were conducted using a BioLogic potentiostat VMP-300. In order to confirm that FTacV can be carried out by commercially available hardware, it was initially evaluated with the well-known reversible $[Ru(NH_3)_6]^{3+/2+}$ redox reaction in an electrochemical cell, with mirror-polished glassy carbon working electrode with a surface area of 0.193 cm^2 (Pine Instruments), an Ag|AgCl (saturated KCl) reference electrode, and a Pt-wire as the counter electrode. The electrolyte was a solution of freshly prepared 0.5 mM $[Ru(NH_3)_6]Cl_3$ (Aldrich, 98%) dissolved in aqueous 0.5 M KCl electrolyte (Acros Organics 99.999%) and was maintained at a room temperature (23 ± 1 °C).

MEA Fabrication

Fuel cell measurements were conducted with homemade membrane electrode assemblies (MEAs). The anode catalyst was prepared by mixing 20% Pt/C (Alfa Aesar) with isopropanol (IP) (Daejung, 99.7%) and 40 wt% D2020 Nafion suspension (Ion Power), up to a concentration of 1 mg/mL, and leaving the suspension under continuous stirring for 24 h. The obtained slurry was then deposited onto a BC29 gas diffusion layer (SGL Group) using an automatic ultrasonic spray machine with a sonication head resonating at 120 kHz (SonoTek Technology), to reach a loading of 0.2 mg Pt/cm^2. The cathode catalyst was prepared by mixing a commercially available Fe-based PGM-free catalyst (Pajarito Powder, PMF-012101) with 35 wt% D2020 Nafion in a 2:1 wt% solution of deionized water (DI) in isopropanol (IPA). The slurry was sonicated for 1 h, stirred overnight, diluted with IPA down to a concentration of 1 mg/mL, and deposited onto the microporous layer of the BC29 electrode. The deposition was carried out using a sonication head resonating at 48 kHz (SonoTek Technology), to reach a loading of 4 mg/cm^2. Both gas diffusion electrodes (GDEs) were weighted after deposition of the catalyst layer and again later after deposition of 0.2 mg/cm^2 layer of Nafion D2020. During the fabrication of the cathode, no PGM containing tools or materials were used. The GDEs and gaskets were then hot-pressed onto a 211NR Nafion membrane (Ion Power) at 130 °C and 2,000 pounds force for 2 minutes.

Fuel Cell Measurements

Fuel cell measurements were performed using an 850e Scribner Associates fuel cell test station. The FTacV and cyclic voltammetry measurements were conducted using BioLogic VMP-300 potentiostat, using two electrodes connected to the anode and cathode of the fuel cell. The fuel cell performance was measured with H_2-O_2 at 80 °C. In fuel cell operating mode, fully humidified H_2 at a flow rate of 100 sccm, and fully humidified O_2 at 125 sccm were supplied to the anode and cathode, respectively, both at a 1.0 bar_g backpressure. Before the measurements, the fuel cell was conditioned for 1 h at a voltage of 0.6 V, after which FTacV and CV measurements were taken. During these measurements, the cathode gas was replaced with N_2. Multiple CVs were cycled prior to the measurements in order to assure that all of the O_2 was purged from the cathode.

Durability tests were conducted at a constant cell voltage of 0.6 V for a series of four one-hour segments. FTacV and CV measurements were taken at the beginning of the experiment and after each segment.

FTacV Measurements

In order for a diagnostic method to work *in situ* PEFC, several guiding principles need to be followed: (1) the method should be easily applicable, preferably electrochemical, (2) the measured signal should be proportional to the activity of the studied catalyst or the density of the electroactive sites, and (3) the response should be distinguishable from other processes in the cell, such as double layer charge/discharge, carbon corrosion, mass transfer, membrane degradation, etc.

The FTacV method has been expanded by A. Bond *et al.* onto new applications over the past couple of decades but it has never been applied in fuel cell research. By now, FTacV has been accepted to be a valuable tool in unraveling complex electrochemical mechanisms,[21-23] and in discerning low-current faradaic reactions from high-current capacitive processes, and high-noise systems.[24-26] An extensive theoretical background has also been developed[21, 25, 27-31]and applied in fully functional electrochemical simulations algorithm, called MECSim, which facilitates the data analysis.[32-34]

Recently, FTacV has been used to de-convolute the electron transfer step in catalytic reaction schemes involving surface-bound inorganic catalysts and enzymes.[35] New insights gained provided important information on the mechanism of electron transfer, which underpins electrocatalytic reactions and enables further catalyst development.[24, 36-41]

FTacV employs a large-amplitude sine wave with a frequency, f, superimposed on a linearly scanned potential ramp. When there are no electroactive species present in the cell, the *ac* current ideally originates only from the capacitance charge/discharge, at the frequency f. On the other hand, when electroactive species are present, the current is a superposition of both non-faradaic and faradaic contributions. Faradaic processes are intrinsically non-linear and generate harmonic components at f, $2f$, $3f$ …nf. This non-linear faradaic current allows for the response in high-order harmonic components to be used to study the electron transfer devoid of other electrochemical processes that take place in parallel. These responses occur at higher frequencies than that of the applied sine wave and are resolved from the fundamental harmonic using FFT to convert the time domain response into the frequency domain, where the higher order harmonics are easily filtered by band selection, as illustrated in Scheme 1. Finally, an inverse FFT algorithm is used to provide the individual harmonics in the time domain. These higher order harmonics are highly sensitive to the reaction kinetics on the electrode and represent only faradaic processes. Hence, these responses are related only to the

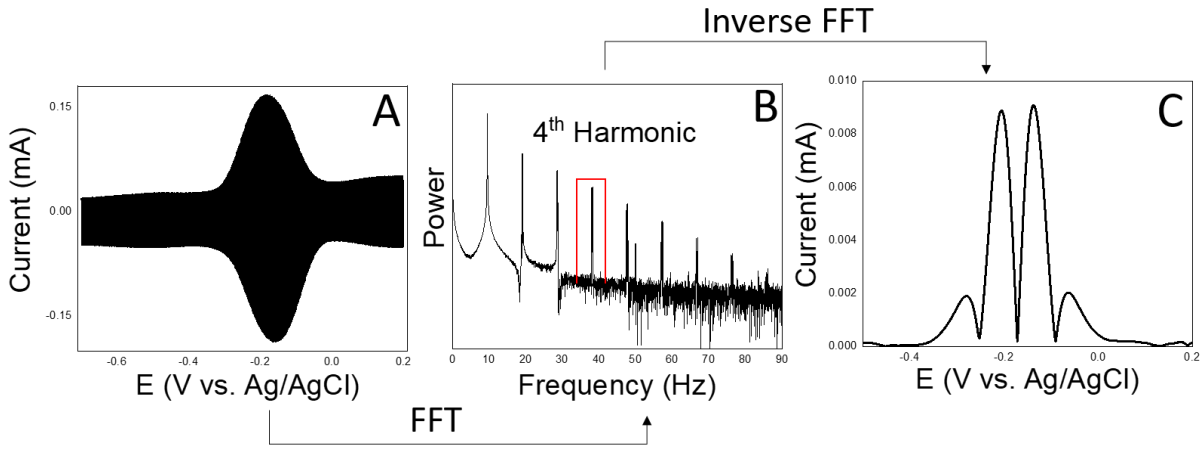

Scheme 1: Scheme representation of data processing for FTacV measurements. The raw current versus time (or potential) data (A) is analyzed via the fast Fourier transform (FFT) algorithm and converted to the frequency domain (B). Each band in the power spectrum is a harmonic in integer multiples of the fundamental harmonic (which is detected at the frequency of the applied sine wave). Each harmonic is selected using a rectangular window (red rectangle in figure 1B), nulling the rest of the harmonics. The filtered harmonic is then transformed back into the time domain via the inverse FFT, where the typical plot is obtained (C being the fourth harmonic in this case). To comply with the Fourier transform requirements, 2^N data points, N being an integer in the range of 1 to 7, were collected per measurement in this work. The frequency, scan rate and data acquisition rate were determined from the equations given in the supplementary information.

active sites that are electrochemically accessible, and not the bulk sites.

Results and Discussion

The main goal of this work was to identify a reliable, active site-specific descriptor for the electrochemical activity of PGM-free ORR catalysts that will allow for monitoring the catalyst degradation during fuel cell testing.

The starting point of this study was a determination whether a commercially available potentiostat could be used for reproducing FTacV experiments reported by Bond *et al.*[42] For this purpose a reversible $[Ru(NH_3)_6]^{3+/2+}$ redox couple and a BioLogic potentiostat were used. Results in Figures S1 and S2 in the SI attest to good agreement with published data obtained in Ref. 38 with custom-made FTacV instrumentation.

MEAs were prepared for fuel cell measurements using commercial Fe-based PGM-free catalysts (Pajarito Powder) at the cathode, and Pt/C at the anode. MEA durability measurements were conducted by holding the fuel cell voltage at 0.6 V for one-hour intervals (Figure S3) and running CV and FTacV measurements in between these intervals. N_2 was used as the cathode gas instead of O_2 in the CV and FTacV measurements. Figure 1 displays CVs measured at the beginning of the measurements and after each durability cycle. The redox peaks associated with the reversible Fe(II)/Fe(III) couple were observed at *ca.* 0.77 V.[18, 20] The CVs taken in between each one-hour hold at 0.6 V showed virtually no change, except for a small increase in peak current as the measurement progresses (black arrows in Figure 1).

While CV excels in general characterization of electrochemical properties, it is not a suitable method for advanced catalyst degradation studies. The error involved in the determination

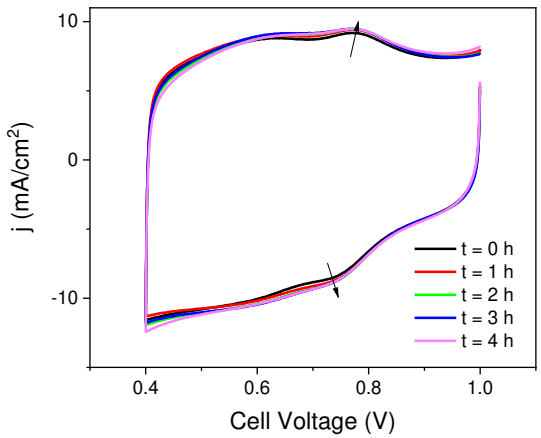

Figure 1: CV of the fuel cell before and after each one-hour 0.6 V hold, at a scan rate of 50 mV/s with fully humidified N_2 at cathode and fully humidified H_2 at the anode.

of charges under the CV current peaks is high due to relatively low faradaic currents compared to large capacitive currents.[20]

In the absence of a catalyst-specific descriptor, fuel cell polarization curves have been the measurement of choice for following degradation of PGM-free catalysts in PEFCs.[18]

The low-current region of fuel cell polarization curves, taken in between the potential holds, is shown in Figure 2. Not surprisingly, fuel cell performance degrades after each one-hour hold at 0.60 V. FTacV measurements were conducted in order to assess changes in the electrochemical activity of the catalytic centers and to distinguish these changes from other possible processes that might have taken place during the durability test.

Figure 3 shows the power spectrum derived from the FTacV measurements, where eight harmonics are evident. Each of the harmonics can be analyzed separately, and compared with other harmonics in order to distinguish between different phenomena occurring at the electrode.[43]

Theoretically, higher harmonics, beyond the 4th, are considered as representative of the non-linear faradaic processes.[44] The potential of the central peak in the odd harmonics and the central minimum in the even harmonics are associated with the reaction potential of the studied redox couple, in this case that of the Fe(III)/Fe(II).[29] Hence, in this work, the 5th, 6th, and 7th harmonics were extracted from the FTacV measurements, all show distinct peaks at a cell voltage of 0.77 V, which have been attributed to the Fe(II)/Fe(III) redox couple in the catalyst layer (Figure 4, gray area), also seen in the CV in Figure 1.

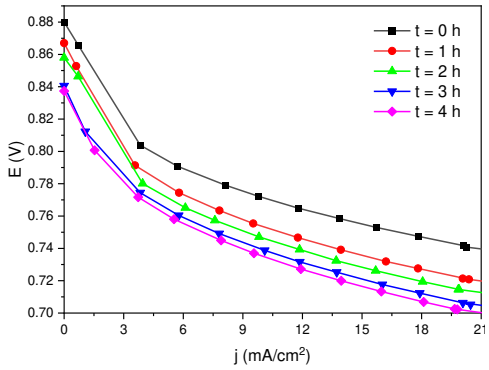

Figure 2: Low current region of the fuel cell polarization curve before and after each one-hour 0.6 V hold. Fully humidified O_2 was supplied at 125 sccm and fully humidified H_2 was supplied at 100 sccm.

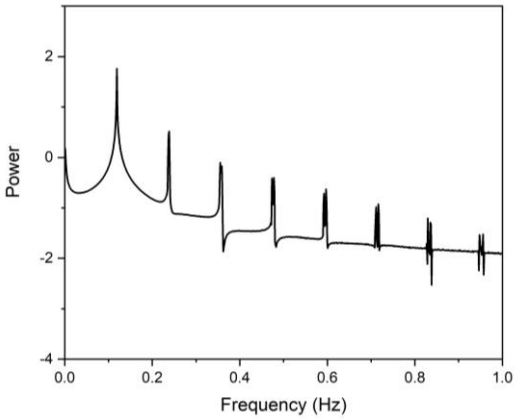

Figure 3: Power spectrum of raw data obtained from FTacV measurments. The power spectrum was obtained by using the FFT algorithm on the data extracted from an FTacV measuremnt which was conducted potentiodynamically in the fuel cell with fully humidified N_2 at cathode and fully humidified H_2 at the anode. Each band of data (the spikes in the figure above) represents an harmonic.

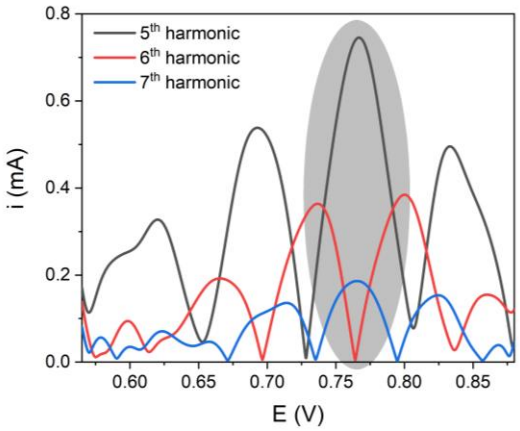

Figure 4: The 5th (black), 6th (red) and 7th (blue) harmonics extracted from an FTacV measurement at the beginning of the measurement. The gray area indicates the cell voltage where all three harmonics minima and maxima coincide showing the formal voltage of the faradaic reaction, which is 0.77 V as seen in the CV in Figure 1. FTacV parameters: initial voltage, $E_i = 0.55\,V$, final voltage, $E_f = 0.9\,V$, frequency of the sine wave, $f = 0.119\,Hz$, amplitude of the sine wave, $\Delta E = 110\,mV$, and the time step for data acquisitions, $dt = 0.4\,ms$. All FTacV measurements were conducted with fully humidified N_2 at cathode and fully humidified H_2 at the anode.

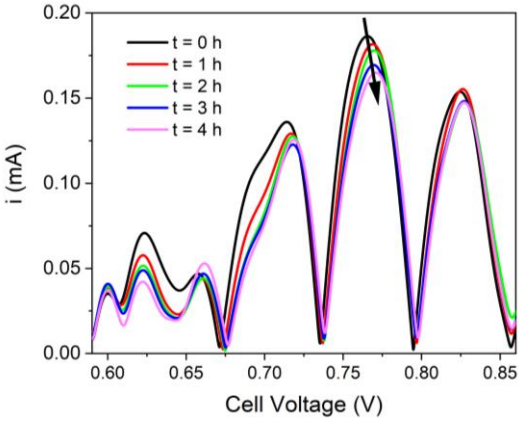

Figure 5: The 7th harmonics generated from FTacV in the fuel cell before and after each hour hold at 0.6 V at different time intervals (t). The experimental parameters are the same as those in Figure 4.

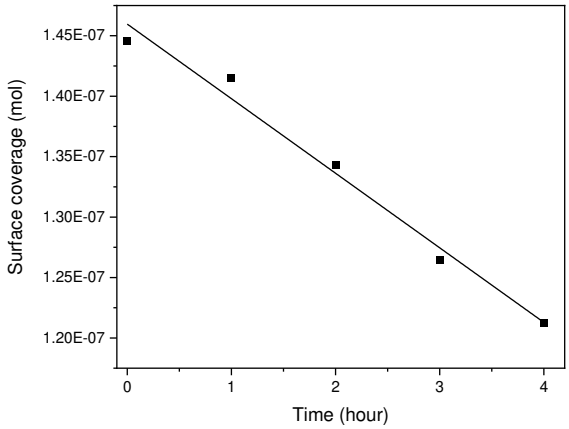

Figure 6: Estimation of the surface coverage of active sites as extracted from FTacV experiment-model comparison over the course of the stability test. The data was fit with a linear model having a slope of $6.2\times 10^{-9}\,mol\,hr^{-1}$ indicating the rate of decay at short times.

The 7th harmonics, measured at the beginning of the experiment and in the intervals between each durability measurement, are shown in Figure 5. These results reveal progressive decay in the peak current at 0.77 V (black arrow in Figure 5) indicating changes in the overall number of accessible electroactive sites and/or to their electroactivity.[24, 45-47]

The absolute amount of electroactive species was heuristically extracted from a model-experiment comparison (Fig. S7). The model employed in this work is that of a single surface confined electroactive species with a surface concentration that follows the Nernst equation with no thermodynamic or kinetic dispersion. For more details on the mathematical model and the numerical methods used in this work, please see references 21, 28-30, 32, 34, 48, 49 and the references therein. The simulation was fitted through trial and error until a reasonable fit was achieved. A value for the heterogeneous rate constant, k^0=2.6 s^{-1}, was found to give the best fit between the simulation and the experimental data of the FTacV measurement conducted at the beginning of life (t=0 hr). The absolute amount of electroactive species used in the simulation was 1.44×10^{-7} moles, corresponding to an EASD of $4.35 \times 10^{18}\,sites\,gr^{-1}$. The change in the total amount of sites during the stability test is plotted in Figure 6. The linear curve fitted to the data indicates that the rate of active-site degradation was constant during the stability measurements, equal to $6.2\times 10^{-9}\,mol\,hr^{-1}$.

The surface coverage of active species decreases by 16.7% during our experiment,

which is lower than the 30% decrease in the current density measured over time at 0.6 V (Fig. S11).

The FeNC catalyst used in this study is expected to have multiple types of Fe centers. It is reasonable to assume that the kinetic and thermodynamic parameters will show some dispersion as each site resides in a different environment. The distribution of the dispersion should change during the fuel cell operation, as different sites are likely to degrade at different rates. The changes seen in the above-mentioned parameters (Table S2), although small, indicate that this indeed may be the case. The use of FTacV can clear a path towards an understanding of degradation mechanisms of various catalytic active sites. Ongoing research in our laboratories, involving less heterogeneous FeNC catalysts with atomically dispersed Fe sites and molecular catalysts, has focused on this highly relevant topic.[50]

Conclusions

In this work, large-amplitude FTacV, a well-established electrochemical method with distinct advantages over *dc* methods, was utilized to follow degradation processes that PGM-free catalysts undergo during fuel cell operation. It was shown that the peak currents from higher harmonics are correlated to the performance of the fuel cell, and that following durability tests they decrease in a manner indicating that the electroactive site loss may not be the only catalyst degradation mechanism, thus inviting more advanced studies of the yet unknown degradation pathway(s). Further work is underway in our laboratories, focusing on the effect of various cathode operation conditions, including correlations between the harmonics' peak currents and the reaction kinetics on different active sites.

Acknowledgments

The Israeli authors would like to thank the Israeli Science Foundation for its support. One of the authors, AF, would like to thank the Israeli Ministry of Energy for his fellowship. Part of this work was conducted under the framework of the Israeli Fuel Cells Consortium (part of Israel National Center for Electrochemical Propulsion). This research was supported in part by a U.S. Department of Energy (DOE) Office of Energy Efficiency and Renewable Energy (EERE), Hydrogen and Fuel Cell Technologies Office (FHTO).

Data availability statement

The authors declare that the data supporting the findings of this study is available within the paper and its supplementary information files.

Code availability

All of the codes and algorithms used for this work are free and will be provided upon request. Please contact either A. Bond (alan.bond@monash.edu), R. Snitkoff (rafisnitkoff@gmail.com) or L. Elbaz (lior.elbaz@biu.ac.il).

References

1. Cano, Z. P.; Banham, D.; Ye, S.; Hintennach, A.; Lu, J.; Fowler, M.; Chen, Z. *Nature Energy* **2018,** 3, (4), 279.
2. He, Y.; Liu, S.; Priest, C.; Shi, Q.; Wu, G. *Chemical Society Reviews* **2020,** 49, (11), 3484-3524.
3. Martinez, U.; Holby, E. F.; Babu, S. K.; Artyushkova, K.; Lin, L.; Choudhury, S.; Purdy, G. M.; Zelenay, P. *Journal of The Electrochemical Society* **2019,** 166, (7), F3136-F3142.
4. Thompson, S. T.; Wilson, A. R.; Zelenay, P.; Myers, D. J.; More, K. L.; Neyerlin, K.; Papageorgopoulos, D. *Solid State Ionics* **2018,** 319, 68-76.
5. Thompson, S. T.; Papageorgopoulos, D. *Nature Catalysis* **2019,** 2, (7), 558-561.
6. Shao, Y.; Dodelet, J. P.; Wu, G.; Zelenay, P. *Advanced Materials* **2019**, 1807615.

7. Banham, D.; Ye, S.; Pei, K.; Ozaki, J.-i.; Kishimoto, T.; Imashiro, Y. *Journal of Power Sources* **2015,** 285, 334-348.
8. Martinez, U.; Babu, S. K.; Holby, E. F.; Zelenay, P. *Current Opinion in Electrochemistry* **2018**.
9. Thompson, S. T.; Wilson, A. R.; Zelenay, P.; Myers, D. J.; More, K. L.; Neyerlin, K. C.; Papageorgopoulos, D. *Solid State Ionics* **2018,** 319, 68-76.
10. Zagal, J. H.; Bedioui, F., *Electrochemistry of N4 macrocyclic metal complexes*. Springer: 2016; Vol. 2.
11. Banham, D.; Ye, S. *ACS Energy Letters* **2017,** 2, (3), 629-638.
12. Martinez, U.; Babu, S. K.; Holby, E. F.; Zelenay, P. *Current Opinion in Electrochemistry* **2018,** 9, 224-232.
13. Meier, J. C.; Galeano, C.; Katsounaros, I.; Witte, J.; Bongard, H. J.; Topalov, A. A.; Baldizzone, C.; Mezzavilla, S.; Schueth, F.; Mayrhofer, K. J. J. *Beilstein Journal of Nanotechnology* **2014,** 5, 44-67.
14. Mayrhofer, K. J. J.; Strmcnik, D.; Blizanac, B. B.; Stamenkovic, V.; Arenz, M.; Markovic, N. M. *Electrochimica Acta* **2008,** 53, (7), 3181-3188.
15. Jia, Q.; Liu, E.; Jiao, L.; Pann, S.; Mukerjee, S. *Advanced Materials* **2019,** 31, (31), 1805157.
16. Jia, Q.; Ramaswamy, N.; Tylus, U.; Strickland, K.; Li, J.; Serov, A.; Artyushkova, K.; Atanassov, P.; Anibal, J.; Gumeci, C. *Nano Energy* **2016,** 29, 65-82.
17. Malko, D.; Kucernak, A.; Lopes, T. *Nature Communications* **2016,** 7, 13285.
18. Osmieri, L.; Ahluwalia, R. K.; Wang, X.; Chung, H. T.; Yin, X.; Kropf, A. J.; Park, J.; Cullen, D. A.; More, K. L.; Zelenay, P. *Applied Catalysis B: Environmental* **2019,** 257, 117929.
19. Tylus, U.; Jia, Q.; Strickland, K.; Ramaswamy, N.; Serov, A.; Atanassov, P.; Mukerjee, S. *The Journal of Physical Chemistry C* **2014,** 118, (17), 8999-9008.
20. Yin, X.; Zelenay, P. *ECS Transactions* **2018,** 85, (13), 1239-1250.
21. Bond, A. M.; Elton, D.; Guo, S.-X.; Kennedy, G. F.; Mashkina, E.; Simonov, A. N.; Zhang, J. *Electrochemistry Communications* **2015,** 57, 78-83.
22. Zhang, Y.; Simonov, A. N.; Zhang, J.; Bond, A. M. *Current Opinion in Electrochemistry* **2018,** 10, 72-81.
23. Ma, H. Mechanistic Electrochemistry: Investigations of Electrocatalytic Mechanisms for H2S Detection Applications. University of Cambridge, 2017.
24. Zhang, Y.; Chen, L.; Li, F.; Easton, C. D.; Li, J.; Bond, A. M.; Zhang, J. *ACS Catalysis* **2017,** 7, (7), 4846-4853.
25. Stevenson, G. P.; Lee, C.-Y.; Kennedy, G. F.; Parkin, A.; Baker, R. E.; Gillow, K.; Armstrong, F. A.; Gavaghan, D. J.; Bond, A. M. *Langmuir* **2012,** 28, (25), 9864-9877.
26. Adamson, H.; Robinson, M.; Bond, P. S.; Soboh, B.; Gillow, K.; Simonov, A. N.; Elton, D. M.; Bond, A. M.; Sawers, R. G.; Gavaghan, D. J. *Analytical chemistry* **2017,** 89, (3), 1565-1573.
27. Engblom, S. O.; Myland, J. C.; Oldham, K. B. *Journal of Electroanalytical Chemistry* **2000,** 480, (1-2), 120-132.
28. Gavaghan, D. J.; Bond, A. M. *Journal of Electroanalytical Chemistry* **2000,** 480, (1-2), 133-149.
29. Lee, C.-Y.; Stevenson, G. P.; Parkin, A.; Roessler, M. M.; Baker, R. E.; Gillow, K.; Gavaghan, D. J.; Armstrong, F. A.; Bond, A. M. *Journal of electroanalytical chemistry* **2011,** 656, (1-2), 293-303.
30. Lloyd-Laney, H.; Robinson, M.; Bond, A.; Parkin, A.; Gavaghan, D. **2020**.
31. Lloyd-Laney, H.; Robinson, M.; Hewson, A. R.; Firth, J.; Zhang, J.; Bond, A.; Parkin, A.; Gavaghan, D.; Yates, N.; Elton, D. **2020**.
32. Kennedy, G. F.; Bond, A. M.; Simonov, A. N. *Current Opinion in Electrochemistry* **2017,** 1, (1), 140-147.
33. Nardis, S.; Mandoj, F.; Stefanelli, M.; Paolesse, R. *Coordination Chemistry Reviews* **2019,** 388, 360-405.

34. Robinson, M.; Ounnunkad, K.; Zhang, J.; Gavaghan, D.; Bond, A. *ChemElectroChem* **2018,** 5, (23), 3771-3785.
35. Adamson, H.; Bond, A. M.; Parkin, A. *Chemical Communications* **2017,** 53, (69), 9519-9533.
36. Adamson, H.; Simonov, A. N.; Kierzek, M.; Rothery, R. A.; Weiner, J. H.; Bond, A. M.; Parkin, A. *Proceedings of the National Academy of Sciences* **2015,** 112, (47), 14506-14511.
37. Chen, L.; Li, F.; Bentley, C. L.; Horne, M.; Bond, A. M.; Zhang, J. *ChemElectroChem* **2017,** 4, (6), 1402-1410.
38. Fleming, B. D.; Zhang, J.; Elton, D.; Bond, A. M. *Analytical chemistry* **2007,** 79, (17), 6515-6526.
39. Guo, S.-X.; Liu, Y.; Bond, A. M.; Zhang, J.; Karthik, P. E.; Maheshwaran, I.; Kumar, S. S.; Phani, K. L. N. *Physical Chemistry Chemical Physics* **2014,** 16, (35), 19035-19045.
40. Lee, C.-Y.; Bond, A. M. *Analytical chemistry* **2008,** 81, (2), 584-594.
41. Li, J.; Bond, A. M.; Zhang, J. *Electrochimica Acta* **2015,** 178, 631-637.
42. Zhang, J.; Guo, S.-X.; Bond, A. M.; Marken, F. *Analytical chemistry* **2004,** 76, (13), 3619-3629.
43. Mashkina, E. A.; Simonov, A. N.; Bond, A. M. *Journal of Electroanalytical Chemistry* **2014,** 732, 86-92.
44. Guo, S.-X.; Bond, A. M.; Zhang, J. *Review of Polarography* **2015,** 61, (1), 21-32.
45. Tan, S.-y. Advanced Electrochemical Techniques for Investigating Electron Transfer Kinetics. University of Warwick, 2017.
46. Song, P.; Ma, H.; Meng, L.; Wang, Y.; Nguyen, H. V.; Lawrence, N. S.; Fisher, A. C. *Physical Chemistry Chemical Physics* **2017,** 19, (35), 24304-24315.
47. Zhang, J.; Bond, A. M. *Journal of Electroanalytical Chemistry* **2007,** 600, (1), 23-34.
48. Honeychurch, M. J.; Bond, A. M. *Journal of Electroanalytical Chemistry* **2002,** 529, (1), 3-11.
49. Gundry, L.; Guo, S.-X.; Kennedy, G.; Keith, J.; Robinson, M.; Gavaghan, D.; Bond, A.; Zhang, J. *Chemical Communications* **2021**.
50. Morris, G. P.; Baker, R. E.; Gillow, K.; Davis, J. J.; Gavaghan, D. J.; Bond, A. M. *Langmuir* **2015,** 31, (17), 4996-5004.

Figures

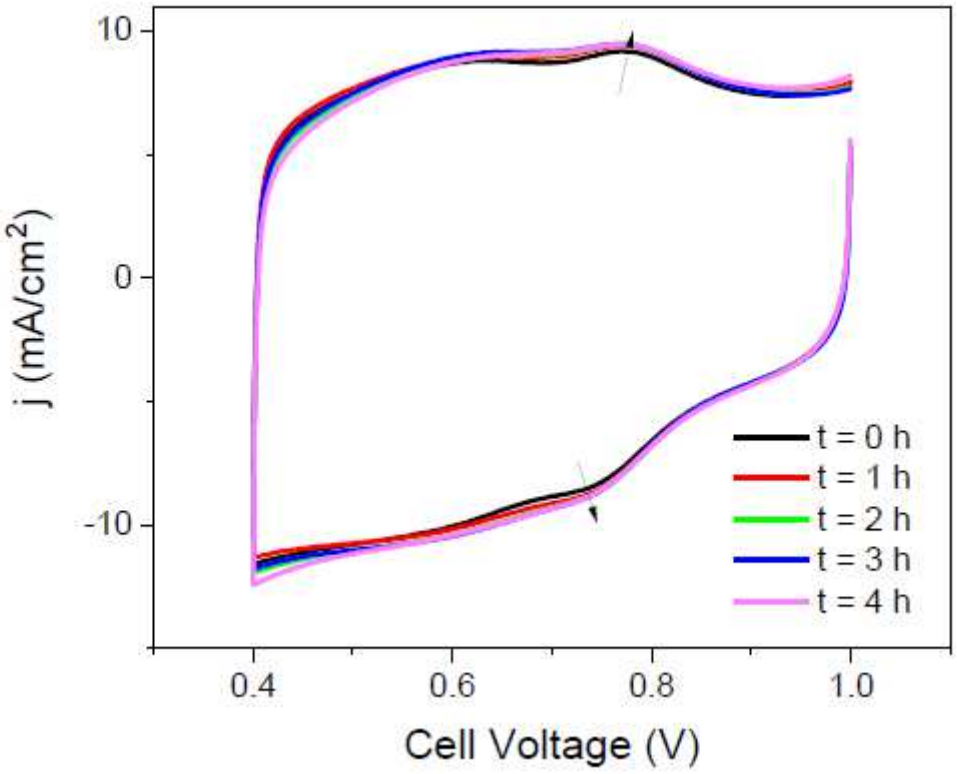

Figure 1

CV of the fuel cell before and after each one hour 0.6 V hold, at a scan rate of 50 mV/s with fully humidified N2 at cathode and fully humidified H2 at the anode.

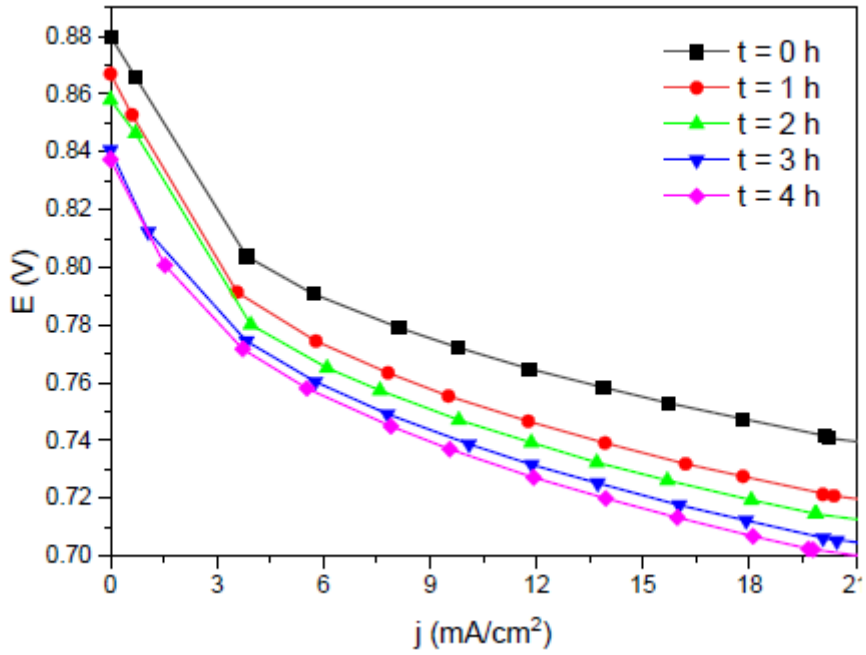

Figure 2

Low current region of the fuel cell polarization curve before and after each one-hour 0.6 V hold. Fully humidified O2 was supplied at 125 sccm and fully humidified H2 was supplied at 100 sccm.

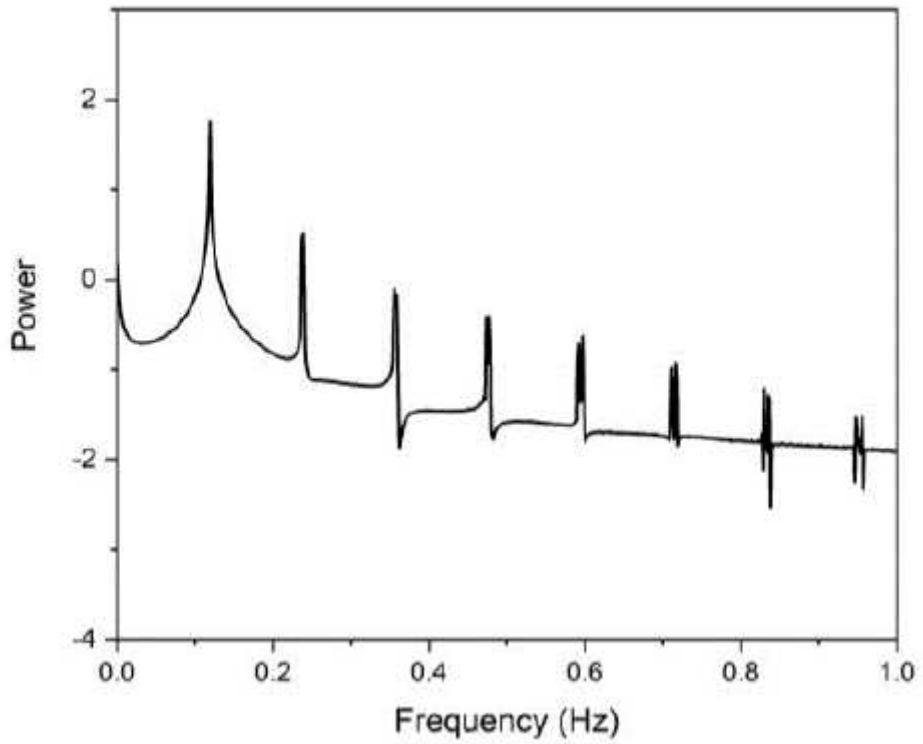

Figure 3

Power spectrum of raw data obtained from FTacV measurements. The power spectrum was obtained by using the FFT algorithm on the data extracted from an FTacV measurement which was conducted potentiodynamically in the fuel cell with fully humidified N2 at cathode and fully humidified H2 at the anode. Each band of data (the spikes in the figure above) represents an harmonic.

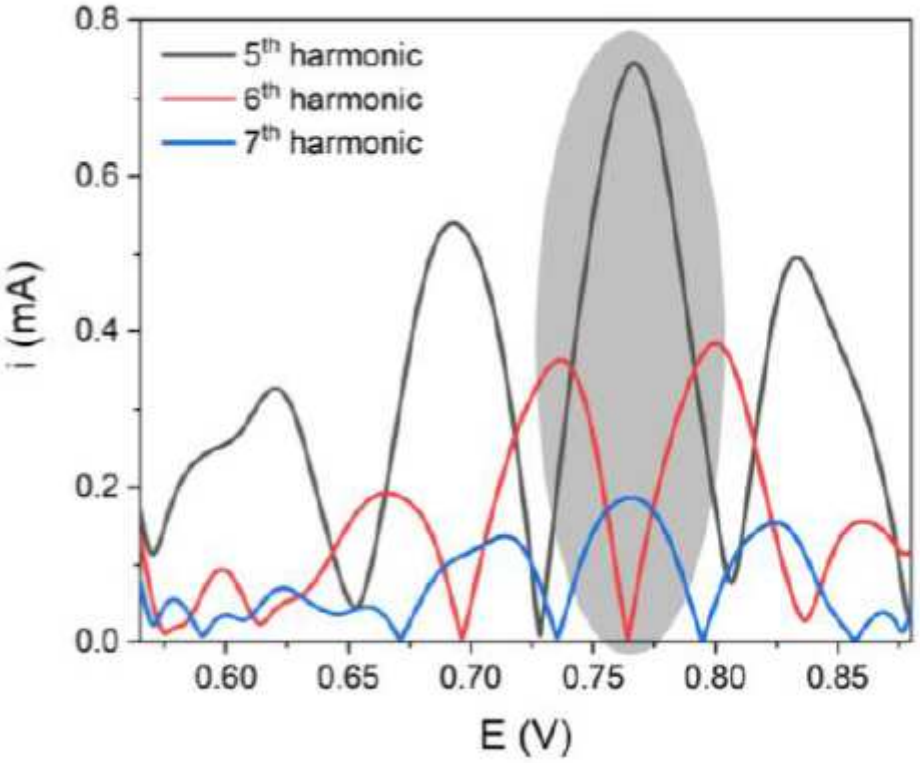

Figure 4

The 5th (black), 6th (red) and 7th (blue) harmonics extracted from an FTacV measurement at the beginning of the measurement. The gray area indicates the cell voltage where all three harmonics minima and maxima coincide showing the formal voltage of the faradaic reaction, which is 0.77 V as seen in the CV in Figure 1. FTacV parameters: initial voltage, □□=0.55 □, final voltage, □□=0.9 □, frequency of the sine wave, □=0.119 □□, amplitude of the sine wave, Δ□=110 □□, and the time step for data acquisitions, □□=0.4 □□. All FTacV measurements were conducted with fully humidified N2 at cathode and fully humidified H2 at the anode.

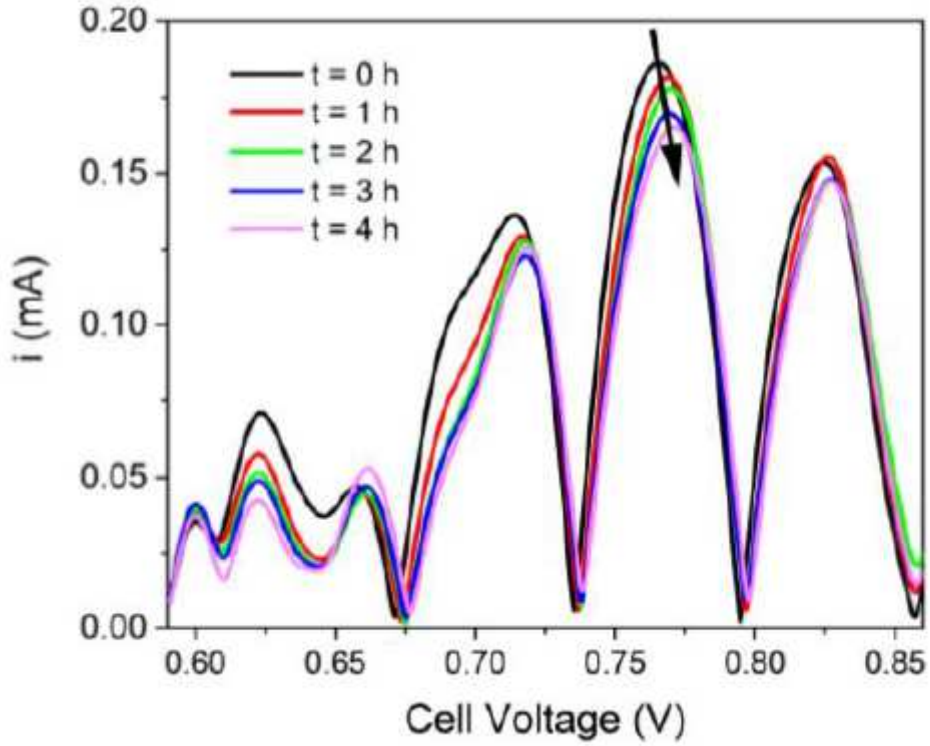

Figure 5

The 7th harmonics generated from FTacV in the fuel cell before and after each hour hold at 0.6 V at different time intervals (t). The experimental parameters are the same as those in Figure 4.

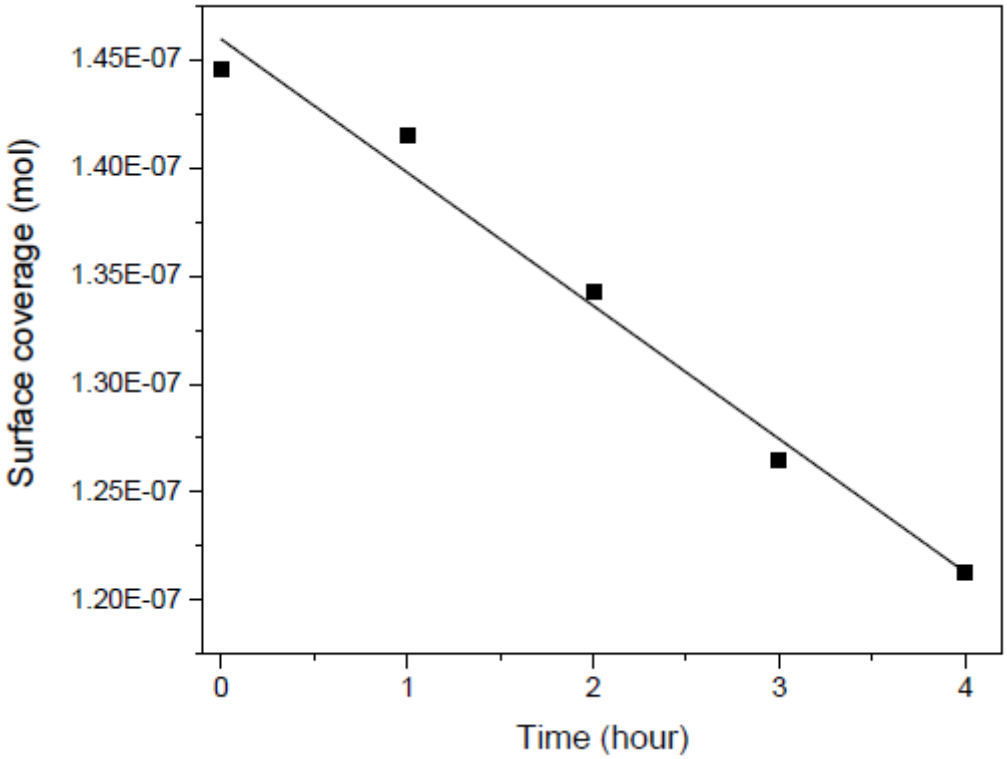

Figure 6

Estimation of the surface coverage of active sites as extracted from FTacV experiment-model comparison over the course of the stability test. The data was fit with a linear model having a slope of 6.2×10−9 □□□ □□−1 indicating the rate of decay at short times.

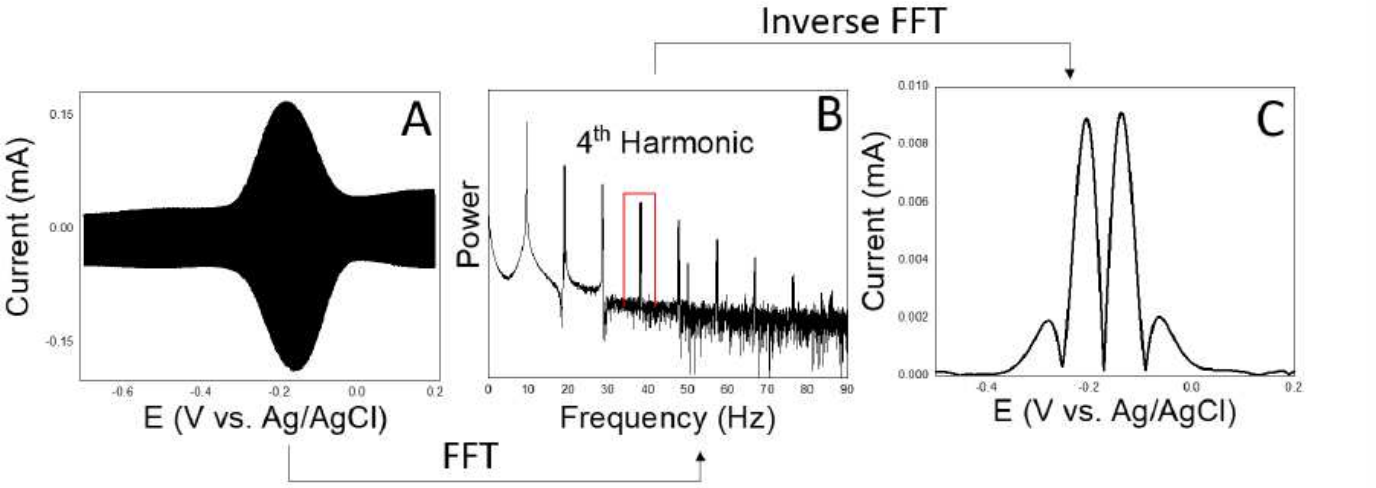

Figure 7

Scheme 1: Scheme representation of data processing for FTacV measurements. The raw current versus time (or potential) data (A) is analyzed via the fast Fourier transform (FFT) algorithm and converted to the frequency domain (B). Each band in the power spectrum is a harmonic in integer multiples of the fundamental harmonic (which is detected at the frequency of the applied sine wave). Each harmonic is selected using a rectangular window (red rectangle in figure 1B), nulling the rest of the harmonics. The filtered harmonic is then transformed back into the time domain via the inverse FFT, where the typical plot is obtained (C being the fourth harmonic in this case). To comply with the Fourier transform requirements, 2N data points, N being an integer in the range of 1 to 7, were collected per measurement in this work. The frequency, scan rate and data acquisition rate were determined from the equations given in the supplementary information.

Supplementary Files

This is a list of supplementary files associated with this preprint. Click to download.

- FTacVSIFinalversion.pdf